Canadian Conference - Pacific Conference on Earthquake Engineering 2023

Vancouver, British Columbia

June 25th – June 30th, 2023

Behaviour of a Reinforced Concrete Shear Wall Subjected to Combined Lateral and Axial Loading

Alessandro Paglia[1*], Austin Martins-Robalino[2], and Dan Palermo[3]

[1]MASc. Student, Department of Civil Engineering, York University, Toronto, ON, Canada
[2]PhD Student, Department of Civil Engineering, York University, Toronto, ON, Canada
[3]Professor, Department of Civil Engineering, York University, Toronto, ON, Canada
[*] apaglia22@hotmail.com (Corresponding Author)

ABSTRACT

In seismic regions, mid-rise and high-rise Reinforced Concrete (RC) buildings are routinely designed to incorporate shear walls to resist seismic excitations and other lateral loading. Typically, ground floor shear walls experience most of the damage during seismic events while also supporting significant self-weight of the structure. Experimental research on shear walls does not always include gravity loading in loading protocols and thus cannot capture the effect of axial loading. Axial loading in slender shear walls has been known to increase the lateral stiffness, reduce cracking along the height of the wall, reduce crack width once the lateral excitation is removed, and aid in re-centering. The following experimental study is focused on quantifying such effects in a RC slender shear wall that is compared to previously tested walls of similar dimensions and construction. The walls in question, measuring 2200 mm high, 1000 mm long, and 150 mm thick, have been used as control walls for experimental testing of slender shear walls reinforced with Shape Memory Alloys (SMAs). This experimental study subjected a steel-reinforced RC shear wall to reverse cyclic lateral loading while maintaining an applied axial load equal to 10% of the wall's compressive capacity. The choice of 10% axial load was based on an upper bound of axial loading for slender shear walls to assess the impact on re-centering. Understanding the behaviour of shear walls to combined lateral and axial loading can aid in better design methods for improving recentering capabilities of RC structures within seismic regions. This study will serve as a control wall for a larger experimental program that will investigate the behaviour of RC shear walls incorporating emerging materials and subjected to combined lateral and axial loading.

Keywords: Reinforced Concrete, Shear Walls, Axial Loading, Lateral Loading, Seismic

INTRODUCTION

In reinforced concrete structures, gravity loading due to self-weight and dead and live loads can impact the response to lateral excitations. Higher axial loading results in higher lateral strength and stiffness but comes at the expense of reduced lateral displacement ductility. In addition, axial loading imposes greater overturning moments at larger displacements through the P-D effect. Understanding the impact of axial loading on the response of slender shear walls was the basis for this research.

Previous research by Abdulridha [1] and Morcos [2] provided experimental test results on slender shear walls subjected to reverse cyclic lateral loading. The walls were similar in design but were not subjected to axial loading during testing. Investigating the effects of axial loading on a reinforced concrete slender shear wall and comparing it to the above previous testing is the focus of this paper. In typical structures with slender shear walls, 10% axial loading represents a high level of axial loading. Thus, the testing conducted in this study provides the response of a shear wall with high axial loading in comparison to previous walls with no axial loading, providing comparisons between the upper bound and lower bound impacts of axial loading.

Specifically, this paper will present the lateral load-lateral displacement response, cracking behavior, yield point, lateral displacement recovery, rotation, and shear strains, and provide a comparison to previous testing. This data will inform future testing of shear walls incorporating emerging materials such as Engineered Cementitious Composite (ECC) and Shape Memory Alloy (SMA) under combined loading conditions. Recent research has reported on the response of slender shear walls repaired with ECC with and without SMA bars [3]. The study, however, did not consider the effect of axial loading.

BACKGROUND

The wall tested in this study is part of a larger experimental program that includes previous research by Abdulridha [1] and Morcos [2]. Both Abdulridha [1] and Morcos [2] constructed and tested a pair of slender shear walls: a control RC shear wall, and a wall containing SMA bars in the boundary regions of the plastic hinge zone.

The RC shear wall (Wall W1-SR) tested by Abdulridha had a height of 2200mm, a width of 1000mm, and a thickness of 150mm. The wall was secured to the laboratory floor via a foundation block and lateral loading was applied to a 400mm x 400mm x 1700mm cap beam. Four pairs of starter bars were included along the base of the wall and extended 300 mm into the foundation and terminated at a height of 300mm above the base. The intent of these bars was to prevent shear sliding at the base of the wall, which can occur in walls with low to no axial loading. The inclusion of these starter bars localized the damage to the top of the starter bars. The final crack pattern and damage in Wall W1-SR (Figure 1 (a)) included flexure-shear cracking pattern and crushing of concrete at the top of the starter bars.

Tests conducted by Morcos [2] expanded the work of Abdulridha. The RC shear wall (Wall SWS-R) constructed by Morcos maintained the same wall dimensions and reinforcement design, however starter bars were not provided in Wall SWS-R. Removing the starter bars resulted in increased cracking along the base of the wall leading to base sliding and rocking; and more horizontal cracking through the web (Figure 1 (b)). The overall crack pattern of Wall SWS-R was predominately flexure with some diagonal cracking in the web. The response of the wall was influenced by the rocking and sliding at the base, which was not present in Wall W1-SR.

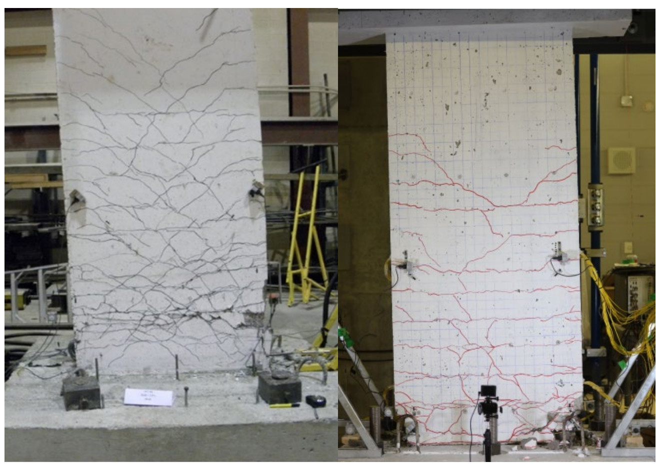

(a) *(b)*

Figure 1. Final crack pattern and damage: (a) Wall W1-SR [1], (b) Wall SWS-R [2].

EXPERIMENTAL PROGRAM

The shear wall in this current study followed the same design implemented by Abdulridha. The wall was named SFW (Shear Wall 5th Edition). The wall shown in Figure 2 had a foundation block that was 500mm deep, 1600mm long, and 1000mm wide, with six anchorage points. The length and width of the foundation block was in accordance with the strong floor perforations of 600mm center to center that provided the anchorage points.

The cap beam measured 590mm deep, 520mm wide and 1200mm long and was slightly larger than the original size to accommodate the larger actuators required to impose the lateral and axial loading. The cap beam included four holes to allow for anchorage to the lateral load applying actuator, and four threaded rods were cast into the top of the cap beam at the mid-length of the cap beam to allow the head of the axial load applying actuator to be securely connected to the top of the cap beam. The wall had a height of 2200mm, a thickness of 150mm and a length of 1000mm. The concrete cover for the foundation and cap beam were 50mm and the cover for the wall was 20mm.

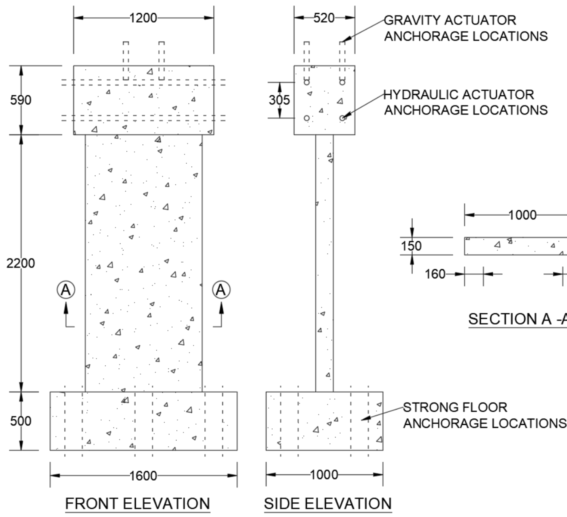

Figure 2. Dimensions of SFW (in millimeters).

Prior to building the wall reinforcement cage, the vertical bars in the boundary region, half of the vertical bars in the web, and three stirrups were equipped with a total of 33 strain gauges. The wall cage consisted of 14-10M vertical bars, four in each boundary region, and six in the web region. The stirrups were placed at a spacing of 150mm c/c from the base of the wall along the entire height of the wall and enclosed all vertical reinforcement. In the boundary region, ties were placed around the four vertical boundary bars to provide additional resistance to buckling. The ties were placed at 75mm c/c up to 1100mm from the base after which they were spaced at 150mm c/c to the top of the wall. In the cap beam, a combination of straight 10M bars and U-shaped 10M bars were used in the reinforcing cage. Figure 3 provides the reinforcement layout of Wall SFW.

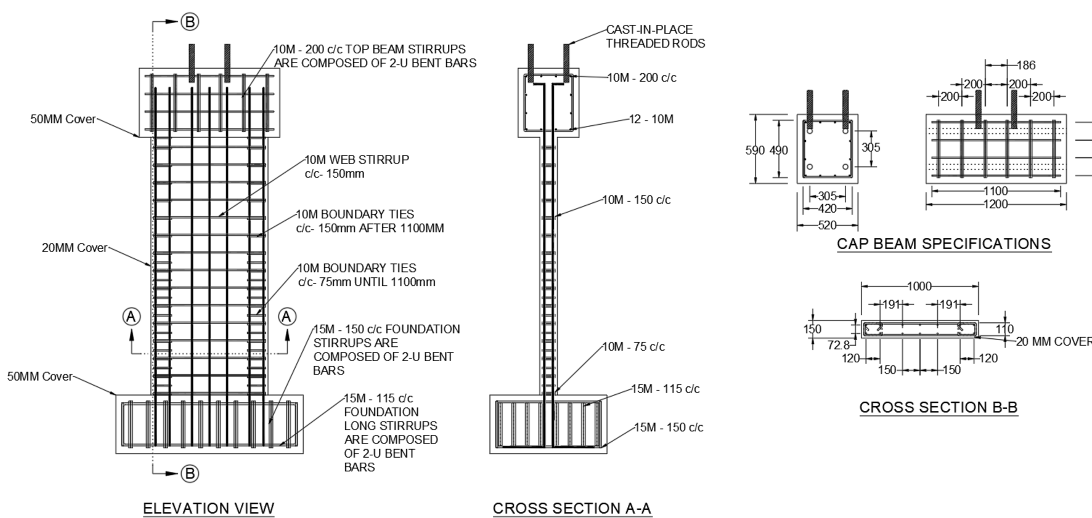

Figure 3. Reinforcement details for SFW.

The lateral loading protocol was a modified version of the displacement-controlled ATC-24 protocol (Table 1). The displacement targets were monitored with a cable potentiometer placed at the mid-height of the cap beam and attached to a frame that was mounted on the foundation block. This provided a direct measurement of the lateral displacement of the wall at the mid-height of the cap beam with respect to the foundation and ensured that any potential sliding or rocking of the foundation did not affect the displacement readings. The loading protocol was based on the drift of the wall. From 0.05% drift (1.25mm) to 1.0% drift (25mm), three repetitions were imposed. After 1.0% drift, two repetitive cycles were imposed to the end of testing.

Table 1. Loading Protocol for SFW.

No.	Drift (%)	Displacement (mm)	Cycles
1	0.05	1.25	3
2	0.1	2.5	3
3	0.2	5	3
4	0.3	7.5	3
5	0.4	10	3 (yield @ 0.37%)
6	0.5	12.5	3
7	1	25	3
8	1.5	37.5	2
9	2	50	2
10	2.5	62.5	2
11	3	75	2
12	3.5	87.5	2
13	4	100	2

EXPERIMENTAL RESULTS

The concrete compressive strength for the wall and cap beam on the day of testing was 38.3 MPa, based on an average of four cylinders. The yield and ultimate strengths of the 10M reinforcement were 440 MPa and 597 MPa, respectively. The constant axial load applied during testing by the vertical actuator was 10% of the wall's compressive capacity ($0.10\,f'_c\,A_g$) resulting in a load of 575kN. The lateral load-lateral displacement response of Wall SFW is shown in Figure 4.

Within the load-displacement response, rupturing of 5 vertical bars is denoted. All four of the exterior boundary vertical bars ruptured and one interior vertical boundary bar ruptured. The exterior boundary bars on the back face of the wall ruptured during the second repetition to the 2.5% drift (62.5mm) cycle and this determined the ultimate displacement of the wall. The global yield point of the wall was 0.37% drift (9.2mm), established using the Park Method [4]. Rupture of the vertical bars along one face of the wall prior to the other face was due to out-of-plane displacements in the wall during testing caused by a leveling issue when casting the cap beam. Testing continued beyond 2.5% drift to observe the post-ultimate response of the wall. During the first 3.0% drift (75mm) cycle, both front face exterior vertical boundary bars ruptured. An attempt was made to push the wall to 3.5% drift (87.5mm) where one interior boundary vertical bar ruptured. The loading was subsequently paused and unloaded as the lateral loading at the final bar rupture was less than half of the lateral load at 3.0% drift.

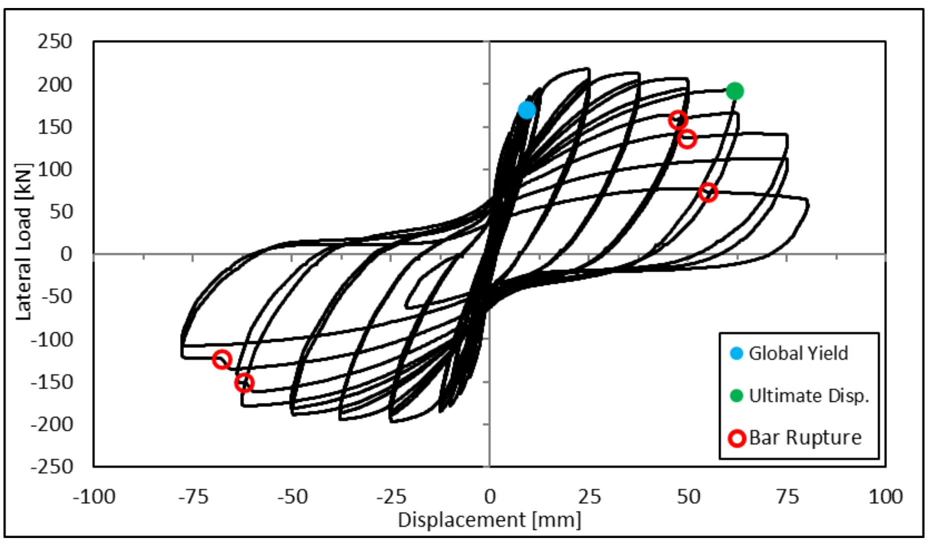

Figure 4. Load-displacement response of SFW.

DISCUSSION

Lateral Load-Drift Envelope Response

Figure 5 illustrates the envelope of the lateral load-drift response of each wall (SFW, W1-SR, and SWS-R) for the first cycle in the positive direction of loading. The responses demonstrate that Wall SFW experienced higher lateral loading and increased stiffness than the walls without axial loading. Wall W1-SR sustained higher lateral loading compared to Wall SWS-R, likely due to the starter bars in Wall W1-SR which prevented sliding and rocking at the base of the wall. In addition, the starter bars increased the stiffness at the base of Wall W1-SR and shifted the critical section to the top of the starter bars. Walls SFW and SWS-R show a more pronounced strength degradation after peak load was attained at a lower drift than Wall W1-SR.

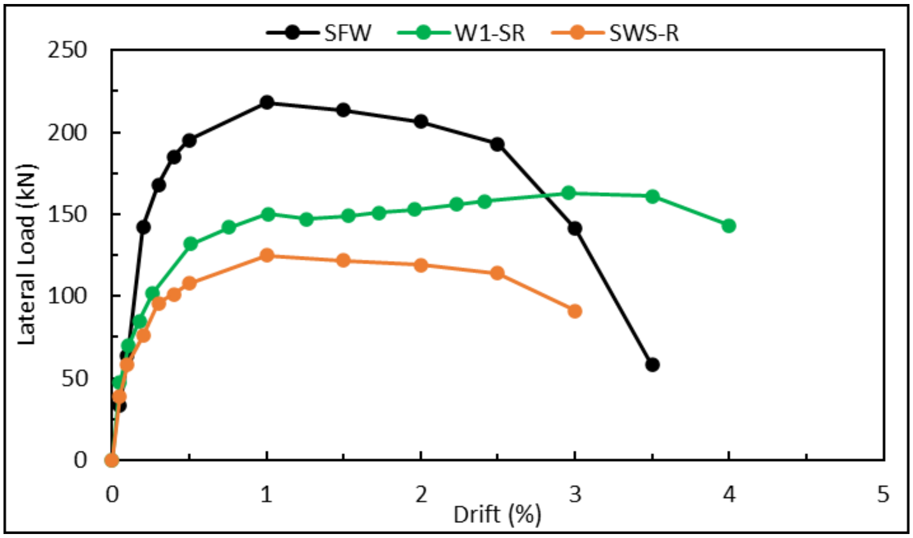

Figure 5. Envelope of lateral load-drift response for positive loading.

Summary of Wall Performance

The first cracking in Wall SFW occurred at 0.20% drift (5mm), and new cracks developed up to 1.0% drift (25mm). After 1.0% drift, no new cracks formed on the wall while existing cracks extended and widened. The majority of cracking occurred within the bottom half (1100mm) of the wall. Cracks were horizontal (flexural) in the boundary regions of the wall and diagonal (shear) in the web region of the wall. Cracks from the base up to 500mm had larger crack width changes during each increase in lateral loading compared to the cracks above 500mm from the base. At the toes in the boundary regions, spalling initiated at 1.0% drift (25mm) and larger pieces spalled off at 2.0% drift (50mm). When the concrete cover was removed, the vertical boundary bars were observed to have buckled prior to rupturing.

Wall W1-SR had four pairs of starter bars to prevent sliding and rocking at the base of the wall. Cracking began at 0.1% drift (2.4mm) in the form of flexural cracks. The wall attained a maximum lateral drift of 4.0% (96mm). On the first negative cycle to this drift level the test was halted. The exterior longitudinal reinforcing bars in the boundary region fractured and significant concrete crushing and longitudinal bar buckling was visible in the opposite boundary region. The average peak load (positive and negative directions) was 156kN at 3.0% drift (72mm). The global yield was determined using the Park Method and was determined to occur at 0.39% drift (9.4mm).

Wall SWS-R first cracked at 0.05% drift (1.2mm) with flexural cracking. Shear cracking formed at 0.2% drift (4.8mm), and the concrete at the right toe experienced crushing at the end of the 2.5% drift cycle (60mm). During the first 3.0% drift (72mm) positive cycle, the two outer boundary bars on the tension side of the wall ruptured. The exposed bars at the opposite boundary region (compression side) had buckled. On the subsequent 3.0% negative cycle, the two outer boundary bars on the tension side also ruptured. During the second positive cycle to 3.0% drift the two inner boundary bars on the tension side of the wall also ruptured. During the final negative cycle, the remaining boundary bars did not rupture, however due to a significant loss in stiffness the test was terminated. The ultimate displacement was deemed to be 2.5% drift (60mm) as this was the final cycle prior to bar rupture. Global yield, determined using the Park Method, occurred at 0.36% drift (8.7mm). The average peak load was 118kN at 1.24% drift (30mm).

The average yield drift, average peak lateral loading, average peak load drift, and average ultimate drift of W1-SR, SWS-R, and SFW are summarized in Table 2.

Table 2. Comparison of Performance Points.

Wall ID	Avg. Axial Load (kN)	Avg. Yield Drift (%)	Avg. Peak Load (kN)	Avg. Peak Load Drift (%)	Avg. Ultimate Drift (%)
W1-SR	0	0.39 (9.4mm)	156	2.96 (71mm)	3.5 (84mm)
SWS_R	0	0.36 (8.7mm)	118	1.24 (30mm)	2.5 (60mm)
SFW	575	0.37 (9.2mm)	208	1.0 (25mm)	2.5 (62.5mm)

Crack Comparison

A comparison of the crack patterns of the three walls is shown in Figure 6. No axial load was superimposed on the two previous tests and Wall W1-SR contained starter bars. Wall SFW, with axial loading, had a crack pattern that was predominantly within the plastic hinge region. There were no horizontal cracks that extended from one boundary to the other boundary except for a crack that surfaced along the base of the wall. However, the walls without axial loading experienced horizontal cracks that spanned across the entire length of the wall.

Wall SWS-R without starter bars and axial loading had significant cracking and some concrete crushing along the base leading to sliding and rocking at the base, whereas Wall W1-SR with starter bars and no axial loading experienced the same phenomenon above the base of the wall and at the termination of the starter bars. Wall SFW sustained cracking along the base of the wall however no sliding or rocking was evident. It also had significant crushing at the toes of the wall due to the increased compressive stresses generated from the axial loading.

(a) (b) (c)

Figure 6. Final crack patterns: (a) W1-SR [1], (b) SWS-R [2], and (c) SFW.

Drift Recovery

Figure 7 illustrates the residual drift-peak drift responses for the three walls for the first cycle in both directions of loading. As the peak drift increased, the residual drift of W1-SR and SWS-R followed more of a linear response in comparison to SFW. Note that the responses of W1-SR are not smooth and is probably due to the critical location being at the termination of the starter bars, where some sliding occurred. Wall SFW recorded the smallest residual drift up to 1.5% leak drift; thereafter, Wall W1-SR experienced the least residual drifts with increasing lateral drift. Comparing the two walls without starter bars, Wall SFW, with axial load, recorded smaller drifts than Wall SWS-R.

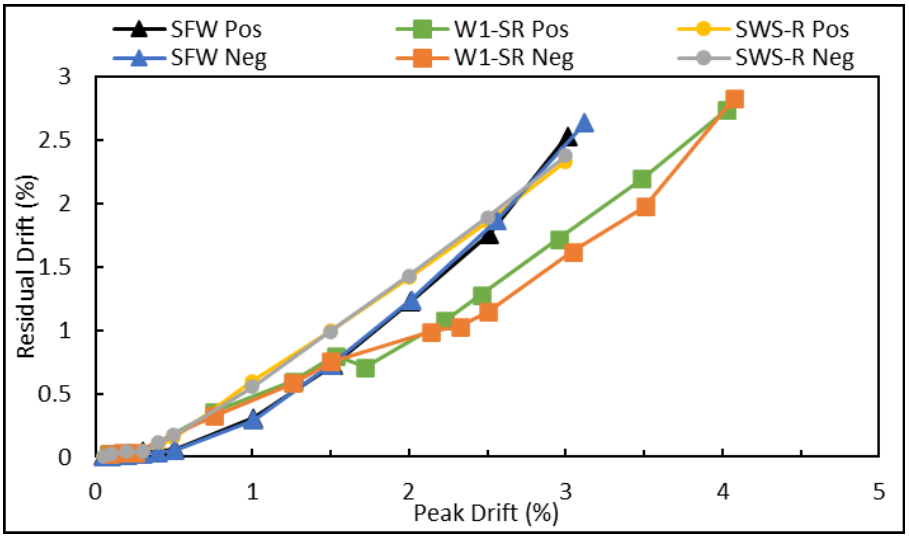

Figure 7. Peak vs residual drift responses.

Figure 8 illustrates the recovery capacity-peak drift response, where the recovery is the displacement that is recovered relative to the peak displacement of a cycle. The recovery capacity of SFW decreased linearly as the lateral drift increased. The trends are similar to the responses in Figure 7; Wall SFW recovered the most lateral displacement up to 1.5% drift, and Wall W1-SR provided the larger recovery beyond 1.5% drift.

The recovery capacity of the walls was similar up to the global yield point of the walls. Beyond yielding significant differences are evident in the response of the walls. At 1.0% drift, W1-SR recovered 54% and SWS-R recovered 42%, while SFW recovered approximately 70%. The recovery capacity at 2.5% drift for SFW and SWS-R were on average 28.5% and 25% respectively. The average recovery capacity at 2.5% drift for W1-SR was 51%, double the recovery capacity of the other two walls. Both SFW and SWS-R recovered roughly 25% prior to the cycle where the first bar ruptured. In Wall W1-SR, the first bar ruptured at 4.0% drift and the recovery capacity of the wall at that point was 31%.

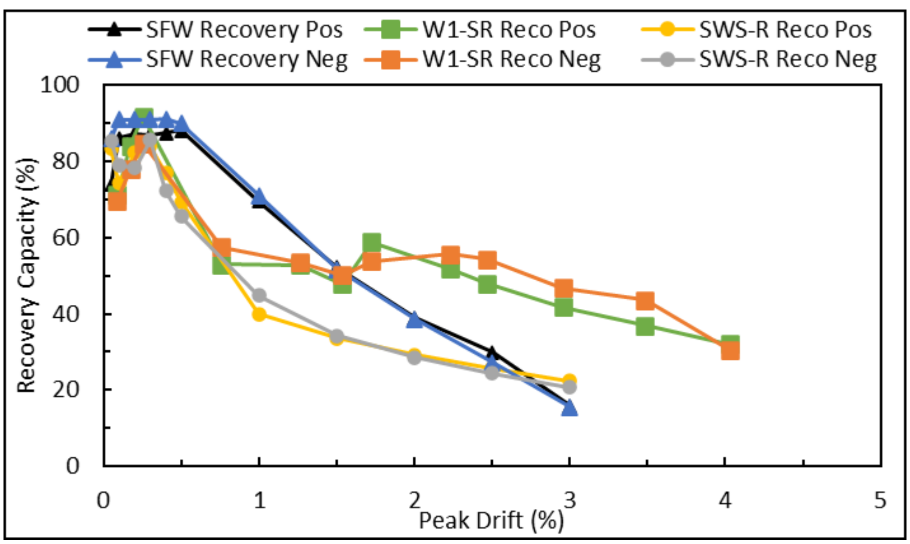

Figure 8. Recovery capacity-peak drift responses.

Wall Rotation

For Wall SFW, the rotation over the full height of the wall (global rotation) was determined from two cable potentiometers (CP7 and CP8) which spanned from the base of the wall to the bottom of the cap beam (Figure 9 (a)). The rotation was calculated from the difference in displacements recorded by the CPs divided by their horizontal distance. CP5 and CP6 measured the vertical displacements at the ends of the wall 100mm above the base. These instruments were also intended to capture potential rocking along the base of the wall. CP9 and CP10 were located within the plastic hinge region, measuring the vertical displacements between 100mm above the base to 950mm above the base. The total rotation over the plastic hinge region was measured by the summation of the rotations measured with CP5 and CP6 and CP9 and CP10 (Figure 9 (b)). It is apparent that most of the wall rotation takes place within the plastic hinge region. Relating back to the crack pattern (Figure 6 (c)), most of the cracking occurred within the plastic hinge region, which aligns with the rotation response. This was not the same for the walls without axial loading as the presence of axial loading contained most of the cracking and rotation within the plastic hinge region.

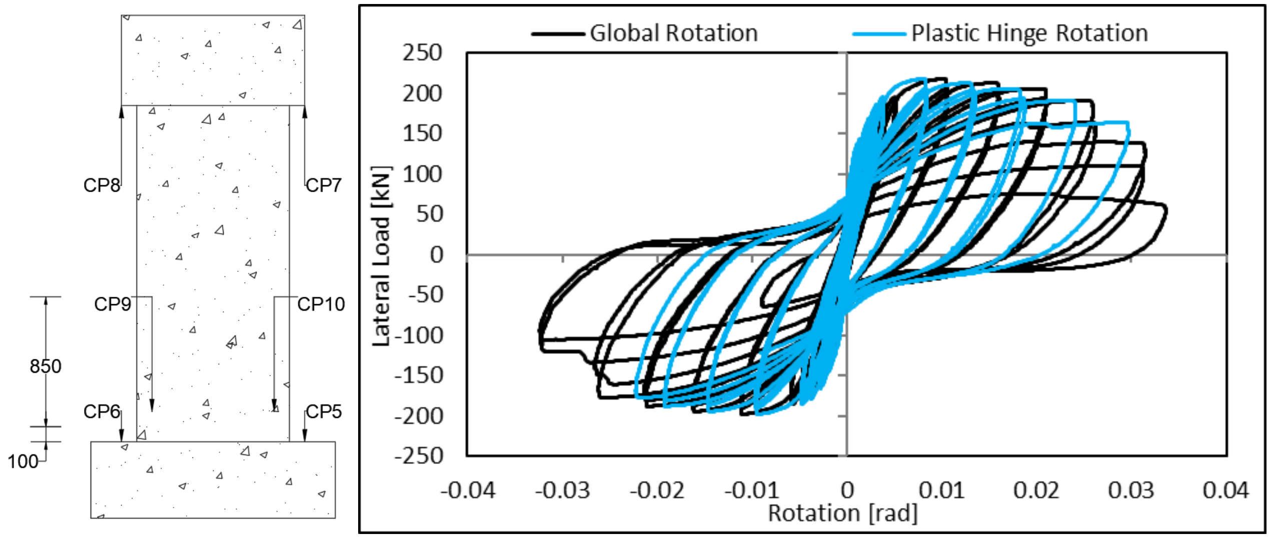

(a) *(b)*

Figure 9. Wall SFW rotation: (a) cable potentiometer locations, and (b) comparison of global and plastic hinge rotations.

Figure 10 depicts the lateral load-global rotation responses of the three walls. [Note, for a comparison of the responses, Figure 10 provides the rotations up to 3.0% lateral drift for all three walls since each wall failed at a different drift.] When comparing the results, Wall SFW experienced greater rotation compared to W1-SR and SWS-R. For this range of data, the rotation curves for SFW are slightly wider than W1-SR and SWS-R. Wall SFW likely experienced more rotation than SWS-R and W1-SR because of the applied axial loading, which controlled other phenomenon such as sliding and rocking that was evident at the base of Wall SWS-R and at the termination of the starter bars in Wall W1-SR. In addition, W1-SR had a different rotation response compared to SWS-R and this can partly be attributed to the rotation of the wall accumulating over a shorter height. Due to the starter bars in W1-SR, there was significant damage accumulation at the top of the starter bars, however below this point, damage was not as severe. The increased stiffness within the region containing the starter bars likely reduced the overall length of the wall that was rotating.

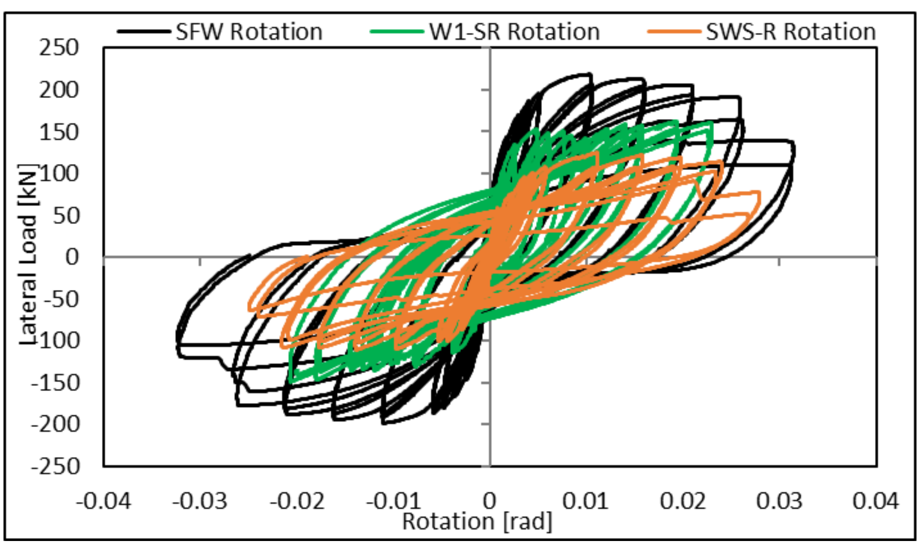

Figure 10. Lateral load-global rotation responses.

Shear Strain

The shear strains within the plastic hinge regions were determined based on Eq. (1) that was reported by Oesterle et al. [5] [6]. In Eq. (1), d is the original diagonal length, δ is the change in diagonal length, h is the original height of the region and l is the original width of the region.

$$\gamma_{avg} = \frac{\delta_1 d_1 - \delta_2 d_2}{2 * h * l} \tag{1}$$

The shear strains were calculated from the displacements captured from CP9-CP12 as shown in Figure 11.

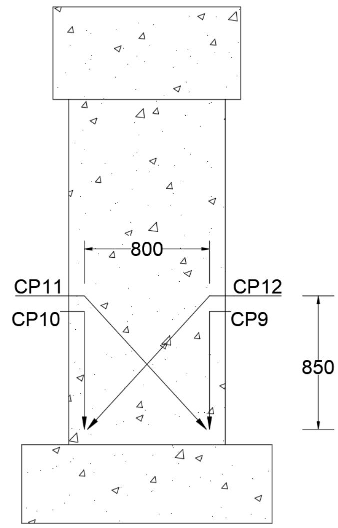

Figure 11. Cable potentiometer locations for SFW for shear strain calculations.

Figure 12 illustrates the shear strain responses of the walls up to 3.0% lateral drift and prior to the accumulation of excessive damage in the plastic hinge regions. The shear strain response for Wall W1-SR was substantially lower than the other walls, which is probably the result of the starter bars that shifted the critical section higher into the wall and increased the stiffness over the bottom 300mm of the wall. Although W1-SR had a well-defined flexure shear crack pattern, it was likely impacted by the starter bars. Walls SWS-R and SFW experienced higher levels of shear strains. Notably, Wall SWS-R experienced ratcheting in one direction; higher shear strains in the positive direction of loading.

At 1.0% drift, Wall SFW experienced shear strains of $1.46\text{x}10^{-3}$ rad and $-1.81\text{x}10^{-3}$ rad in the positive and negatives directions of loading, respectively. At the same drift, Wall SWS-R recorded shear strains of $2.02\text{x}10^{-3}$ and $-2.20\text{x}10^{-3}$. For Wall W1-SR at the same drift, the shear strains were 0.47 $\text{x}10^{-3}$ rad and -0.48 $\text{x}10^{-3}$ rad.

In the positive and negative directions of loading to 2.5% drift, Wall SFW experienced shear strains of $4.40\text{x}10^{-3}$ rad and -4.93 $\text{x}10^{-3}$ rad, respectively. For Wall SWS-R, the shear strains at 2.5% drift were 7.48 $\text{x}10^{-3}$ rad and -6.01 $\text{x}10^{-3}$ rad. Wall W1-SR at 2.5% drift sustained shear strains of $0.972\text{x}10^{-3}$ rad and $-0.566\text{x}10^{-3}$ rad. Wall W1-SR experienced less overall shear strains compared to SWS-R and SFW. Wall SFW experienced less shear strain at 1.0% drift and 2.5% drift than Wall SWS-R.

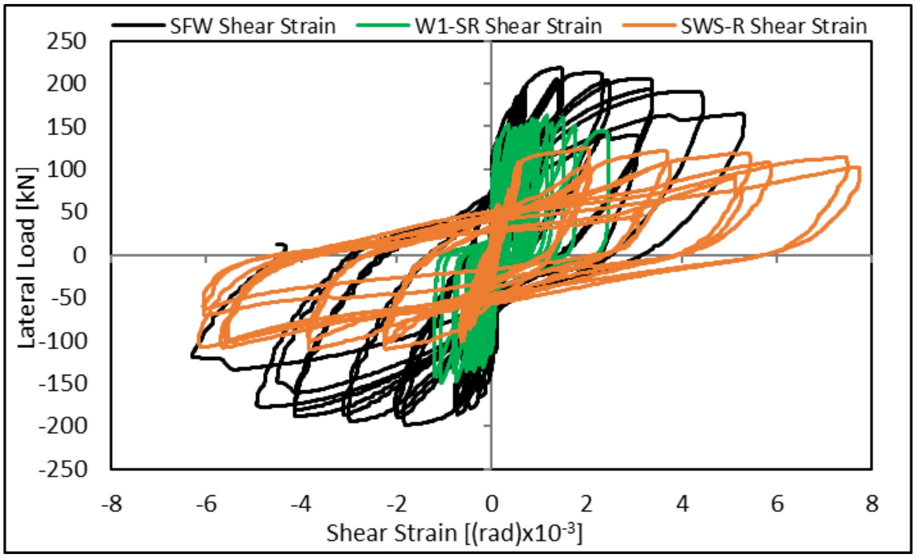

Figure 12. Shear strains in plastic hinge regions.

CONCLUSIONS

The study presented in this paper examined the effects of axial loading on a slender shear wall with similar reinforcement to other walls with no axial loading. The effect on cracking, recovery capacity, global rotation, and shear strains was discussed, and the following conclusions are drawn:

1. The cracking behavior of all walls was predominantly flexure, but the presence of axial loading restricted the propagation of horizontal flexural cracks to the boundary regions. In the wall with axial load, cracking through the web was dominated by shear. The walls had similar flexural-shear crack patterns; however the inclusion of axial loading affected the height over which cracking occurred.
2. In the walls without axial loading, cracking occurred along the entire height of the wall. The wall with axial loading experienced cracking over the bottom half of the wall.
3. Buckling of vertical reinforcement was observed in all three wall tests. The wall with axial loading sustained greater buckling due to the increased compressive stresses.
4. The global yield drift was similar for all three walls. Global yielding of the walls in this study was not affected by the presence of axial loading.
5. The responses of the two walls without axial loading were significantly affected by the presence of starter bars which increased the lateral strength and stiffness, changed the location of the plastic hinge, and reduced the effective height over which the wall was rotating.
6. The recovery capacity of the wall with axial loading was linear after yielding until the end of testing. Axial loading improved the recovery capacity compared to the walls without axial loading up to 1.5 % drift.
7. The rotation response of the walls was improved with the presence of axial loading. Beyond 1.0% drift, the global rotations of the wall with axial loading increased compared to the walls without axial loading.
8. The level of shear straining was similar between Walls SFW and SWS-R. However, Wall SWS-R experienced greater ratcheting in one direction of loading.

This study presented the response of slender shear walls that were well designed and constructed using conventional materials. Understanding the responses of such walls provides a baseline to understanding the response of walls with emerging materials, such as SMA (Shape Memory Alloy) and ECC (Engineering Cementitious Composite) An example of a salient response parameter is the residual drift at the end of a seismic event, which is an important consideration in determining the post-earthquake functionality of a structure. Future testing will consider shear walls with emerging materials to improve the lateral displacement recovery capacity and the damage resilience.

ACKNOWLEDGMENTS

The authors acknowledge the financial support from the NSERC Discovery Grants program.

REFERENCES

[1] A. Abdulridha and D. Palermo. (2017). "Behaviour and Modelling of Hybrid SMA-Steel Reinforced Concrete Slender Shear Wall," *Engineering Structures,* vol. 147, pp. 77-89.

[2] M. Morcos and D. Palermo. (2019) "SMA-Reinforced Concrete Shear Walls Subjected to Reverse Cyclic Loading," in *Fifth Conference on Smart Monitoring, Assessment, and Rehabilitation of Civil Structures (SMAR 2019)*, Postdam, Germany.

[3] M. Soto-Rojas, A. C. Ferche and D. Palermo. (2023). "Behaviour of Shape Memory Alloy-and Steel-Reinforced Shear Walls Repaired with Engineered Cementitious Composite," *ACI Struct J,* accepted March 2023.

[4] R. Park. (1989). "Evaluation of Ductility of Structures and Structural Assemblages from Laboratory Testing," *Bulletin of the New Zealand Society for Earthquake Engineering,* vol. 22, no. 3, pp. 155-166.

[5] R. G. Oesterle, A. E. Fiorato, L. S. Johal, J. E. Carpenter, H. G. Russell and W. G. Corley. (1976). "Earthquake Resistant Structural Walls - Tests of Isolated Walls," Research and Development Construction Technology Laboratories, Portland Cement Association.

[6] R. G. Oesterle, J. D. Aristizabal-Ochoa, A. E. Fiorato, H. G. Russell and W. G. Corley. (1979). "Earthquake resistant structural walls-tests of isolated walls-phase II," Construction Technology Laboratories, Portland Cement Association.